Open Veterinary Journal, (2024), Vol. 14(12): 3569-3580
ISSN: 2226-4485 (Print)
ISSN: 2218-6050 (Online)
Research Article
DOI: *10.5455/OVJ.2024.v14.i12.39*

Submitted: 11/10/2024 Accepted: 18/11/2024 Published: 31/12/2024

Anti-MRSA effects of synergism of recombinant lysostaphin with biosynthesized silver nanoparticles

Zeena Fouad Saleh[1]* and Balsam Miri Mizher[2]

[1]*Unit of Zoonotic Disease Research, College of Veterinary Medicine, University of Al-Qadisiyah, Al-Diwaniyah, Iraq*
[2]*Department of Veterinary of Microbiology, College of Veterinary Medicine, University of Al-Qadisiyah, Al-Diwaniyah, Iraq*

ABSTRACT

Background: Methicillin-resistant *Staphylococcus aureus* (MRSA) strains become a major challenge to public health and health provider due to their wide spread and resistance to wide spectrum of antibacterial agents.

Aim: This study aimed to characterize recombinant lysostaphin produced by *Escherichia coli* BL21(DE3) and to investigate the biosynthesis of silver nanoparticles (SNPs) by *Candida albicans* against MRSA.

Methods: Samples were collected from vaginal samples. The methods included efficient cloning, expression, and purification of recombinant lysostaphin, a potent antibacterial enzyme targeting *S. aureus*, and achieved with advanced molecular techniques in *E. coli* BL21(DE3). The SNPs were synthesized using a biogenic approach with *C. albicans*, demonstrating stable and efficient silver ion reduction, as confirmed by ultraviolet-visible spectroscopy, scanning electron microscope, and Fourier-transform infrared spectroscopy (FTIR) analyses.

Results: The antibacterial assays against MRSA strains of *S. aureus* showed significant inhibition by both lysostaphin and SNPs. The combination of biosynthesized SNPs/polyethylene glycol with lysostaphin exerted significant activity against tested bacteria, resulting in zone of growth inhibition of 20.33 ± 0.88 mm.

Conclusion: These findings suggest a promising synergistic antibacterial strategy, offering hope in the fight against MRSA. The study findings reveal that lysostaphin and SNPs could be effective in the treatment of MRSA-related infections, especially when used in combination.

Keywords: *Candida albicans*, Nanoparticles, Mastitis, Recombinant lysostaphin, Synergistic effect.

Introduction

Methicillin-resistant *S. aureus* (MRSA) strains become a major challenge to public health and health provider due to their wide spread and resistance to wide spectrum of antibacterial agents. Strains belonging to MRSA are major part of hard-to-treat mastitis. Lysostaphin, a metallo-endopeptidase naturally synthesized by *Staphylococcus simulans*, stands out among the latest antimicrobial agents targeting *S. aureus* (Xie *et al.*, 2022). Lysostaphin has unique features, including exceptional steadiness, minimal toxicity, and distinctive preciseness, which make it a promising antibacterial agent (Lekha *et al*., 2021). Previous methods of producing lysostaphin involved purifying it from crude *S. simulans* and *E. coli* extracts, which could contain traces of pyrogens or allergens (Timmerman *et al*., 1993). The mature form of lysostaphin is also separated from the propeptide utilizing *S. simulans* extract (Boksha *et al*., 2016; Ceotto-Vigoder *et al*., 2016; Khandel and Shahi, 2018; Grishin *et al*., 2020; Jayakumar *et al*., 2021).

Nanotechnology emerges as a leading strategy for safeguarding and bolstering the endurance of protein or peptide drugs over extended durations (Khandel and Shahi, 2018). The amalgamation of these compounds offers several advantages: serving as a precision tool for targeting bacteria (Gonçalves *et al*., 2018), mitigating bacterial resistance, shielding antibacterial agents from inhibitors or adverse conditions, and serving as a sustained preservative within pharmaceutical industries (Gomes and Henriques, 2016). The utilization of diverse biological entities rather than hazardous chemicals for nanoparticle downsizing and strengthening has garnered considerable attention. Among the myriads of potential bioresources, biologically active materials derived from yeast and fungus are exceptional platforms for this purpose (Fagundes *et al*., 2010). Yeast and fungus demonstrate remarkable proficiency in secreting extracellular enzymes, and their rapid growth allows

***Corresponding Author:** Zeena Fouad Saleh. Unit of Zoonotic Disease Research, College of Veterinary Medicine, University of Al-Qadisiyah, Al-Diwaniyah, Iraq. Email: *zeena.saleh@qu.edu.iq*

for straightforward culturing and maintenance in laboratory settings (Fang *et al*., 2023). Moreover, they possess the capability to generate metal nanoparticles and nanostructures through intracellular or extracellular enzyme-mediated reduction (Guardabassi *et al*., 2020). As previously mentioned, while antibiotics remain the primary treatment approach for bacterial infection, their efficacy is constrained, further complicated by the rise of pathogen strains resistant to antibiotics, which presents a severe obstacle to antibiotic therapy (Birla *et al*., 2013). Consequently, it is imperative to explore alternative novel therapeutic agents that hold promise for controlling and treating mastitis.

Therefore, this study aimed to explore the production of characterized recombinant lysostaphin produced by *E. coli* BL21(DE3) and to investigate the biosynthesis of silver nanoparticles (SNPs) using *C. albicans* against MRSA.

Materials and Methods

Bacterial isolates

The current study used bacterial stocks of MRSA isolates originally recovered from cow mastitis. These stocks were obtained from the Laboratory of Microbiology, College of Veterinary Medicine, University of Al-Qadisiyah, Al-Diwaniyah City, Iraq.

Cloning of gene encoding lysostaphin

Escherichia coli BL21(DE3) was transformed using chemically competent *E. coli* (C2527) via heat shock method according to the instruction by BioLabs Company (UK). The complete sequence of lysostaphin gene was synthesized using advanced next-generation gene synthesis technology and determined according to Szweda *et al*. (2001) and incorporated into the plasmid cloning vector pET28-a(+) by GenScript (USA), using the unique BamHI and XhoI restriction sites through standard molecular cloning techniques. These enzymes were used by the company to generate the plasmid that was used in the current study to carry the lysostaphin gene and follow the company protocol (Ali and Chew, 2015).

The optimization of isopropyl β-D-1-thiogalactopyranoside (IPTG) inducer for recombinant Lysostaphin gene expression in *E. coli* was conducted using real-time quantitative Polymerase chain reaction (qPCR) assay. *Escherichia coli* cells were induced with different concentrations of IPTG (0.25-, 0.5-, 0.75-, and 1-mM IPTG), and the cycle threshold (CT) values for the recombinant Lysostaphin gene and the housekeeping *16SRNA* gene were measured. Using the RT-qPCR, the concentration 1-mM IPTG was used all over the study.

The ▲CT (average CT) values for the recombinant Lysostaphin gene were calculated by normalizing to the CT value of the housekeeping *16SrRNA* gene. The fold change in gene expression was then compared to the control samples stimulated with 0.25-mM IPTG.

Biomass production of producer strains

In the beginning, different IPTG concentrations were utilized in groups of Luria Bertani (LB) cultures, with the use of the standard bacteria and the plasmid at a single concentration. The mixture was incubated overnight. After using the RT-qPCR, the best IPTG concentration was detected. After 24 hours, the culture of *E. coli* BL21 was mixed with 200 ml of LB and 25-µg/ml kanamycin)Aquascience/USA(and was incubated using a rotary shaker at 200 rpm and 25°C. Then, 1-mM IPTG (Rensselaer Polytechnic Institute, USA) was added to the culture to get 1.0–1.5 OD turbidity, followed by incubation for 4–5 hours. The biomass at 0.5 g/l was collected after 6000-rpm cold centrifugation for 15 minutes (Boksha *et al*., 2016).

Recombinant lysostaphin protein expression

The expression of recombinant lysostaphin protein was optimized at different incubation temperatures (37°C, 30°C, 25°C, and 15°C) and induction conditions with varying concentrations of IPTG (1.0, 0.75, 0.5, and 0.25 mM) for 4–5 hours. This experiment aimed to determine the optimal concentration of IPTG inducer and incubation temperature on *E. coli* BL21(DE3) for lysostaphin expression in order to obtain a large amount of active lysostaphin protein with shaking at 200 rpm. The purified lysostaphin protein was set based on the binding capacity of Ni-charged 100 µl of 30-µm MagBeads (GenScript, USA) to 1-mg His-tagged lysostaphin protein using a 250-mM imidazole (Central Drug House (CDH), India) binding buffer and incubated at 4°C with rotation for 60 minutes (Boksha *et al*., 2016).

Lysostaphin purification

For the purification, *E. coli* BL21 was added to 25-mM Tris-HCl buffer at pH 7.5, 50-mM NaCl, and 1-mM phenylmethylsulfonyl fluoride (PMSF) (Sigma-Aldrich, USA). The next three steps show how to purify 6× His-tagged lysostaphin protein from a cellular level through column chromatography. To start off, cells are resuspended in 20 ml of ice-cold lysis buffer containing 1-mM PMSF, a serine protease inhibitor to prevent the degradation of the recombinant protein during the cell lysis. Then, 181-second bursts of sonication are applied, while the cells are submerged in an ice-cooled water bath, at an intensity of high sonication with a 3-second cooling interval between bursts. During the sonication, optionally, 20 µl of 10-µg/ml ribonuclease A and 50 µl of 5-µg/ml deoxyribonuclease I can be added into the lysate with 3-hour incubation before centrifugation at 4°C to decrease the viscosity of the lysate. After sonication, the mix is centrifuged at 15,000 × gravity for 15 minutes at 4°C to separate the cell debris, and supernatant is collected as a starting material for purification and characterization (Rensselaer Polytechnic Institute, USA). The protein concentration was assessed using the Bradford protein assay (Hema *et al*., 2016). Sodium dodecyl

sulfate (SDS)–polyacrylamide gel electrophoresis (PAGE) is a technique that uses SDS (BioBasic/Canada) and polyacrylamide gel (bioWORLD/USA) for separation of protein molecules according to their molecular weight (kDa). The total extracted crude bacterial protein, purification column flow-through, and washed proteins as well as 6× His-tagged eluted lysostaphin protein were analyzed by the SDS-PAGE technique according to the method described by Rosenberg *et al*. (1996). This assay measured the concentration of extracted and purified total protein from bacteria. Protein electrophoresis was conducted on a 30% polyacrylamide gel (Shahid and Khan, 2020).

Quantitative reverse transcription real-time PCR

The quantitative real-time PCR technique was performed for quantification detection and gene expression analysis of recombinant lysostaphin gene expression in *E. coli* according to the method described by Dong *et al*. (2018).

Data analysis of qPCR

The data results of qPCR for target and housekeeping genes were used for expression analysis (fold change). The ΔCT method used a reference gene that was described by Ivak and Schmittgen (2001) as the following equation:

Ratio (reference/target) = 2CT(reference) – CT(target).

Intracellular biosynthesis of SNPs

Sample collection and laboratory diagnosis

Sterile swabs were utilized to obtain vaginal samples from the Maternity and Children Teaching Hospital in Al Diwaniyah, Iraq. Patients were asked to insert the swab without touching outside the vaginal environment. Each sample underwent a light microscopic (Olympus, Japan) examination, and slides were prepared for Gram staining. Furthermore, samples for fungal culture were introduced into potato dextrose agar (PDA) supplemented with chloramphenicol and gentamicin (Sigma-Aldrich, USA) and subsequently incubated at 30°C. *Candida* species were identified through morphological and physiological methods, including culture on CHROM agar Candida (Ibrahim *et al*., 2021).

Fungal biomass production

The Basavaraja method (Basavaraja *et al*., 2008) was used to produce the SNPs, utilizing *C. albicans* on PDA. The plates were incubated for 3 days at 37°C. Colonies of *C. albicans* were harvested, after the designated incubation period, using an L-shaped spreader with 10 ml of deionized water per plate. The cells were then used to produce SNPs through biosynthesis (Rahimi *et al*., 2016).

Biosynthesis of SNPs

In a 250-ml Erlenmeyer flask, a mixture of 50 ml of *C. albicans* cell suspension and 50 ml of 1 mM $AgNO_3$ solution was created to produce SNPs. After that, this combination was kept at 25°C for 24 hours in a shaking incubator with a 150-rpm setting. A sample of 3 ml was withdrawn at a fixed interval, and the absorbance was taken. The synthesized SNPs were placed on a sterile plate and dried aseptically under laminar airflow (Hamida *et al*., 2021).

Characterization of biosynthesized SNPs

The synthesis of SNPs was monitored by ultraviolet-visible (UV-vis) spectroscopy (SPEKOL 1300, Germany), specifically utilizing a Shimadzu UV Pharma Spec 1700 spectrophotometer of 0.72 nm of a resolution. Then, SNPs underwent examination via scanning electron microscopy (SEM, JEOL JSM 6360, Japan). Particle size analysis was also utilized to determine the precise distribution of the SNPs (Cumberland and Lead, 2009). Fourier transform infrared spectroscopy (FTIR) was employed to examine the SNPs (Faghihzadeh *et al*., 2016).

Polyethylene glycol-coated SNPs

Polyethylene glycol (Vasudha Chemicals/India) (PEG)-coated SNPs (SNPs–PEG) were produced using modified Turkevich's method (Pinzaru *et al*., 2018). SNPs at 2.38-mg⁄ml SNPs were added to 2.38 mg PEG (1:1) (w⁄w) and constantly homogenized. The mixture was then kept in a refrigerator for later use (Pinzaru *et al*., 2018).

Loading of SNPs–PEG and lysostaphin

Lysostaphin–PEG was prepared by adding 2.38 mg of PEG to a 2.38-mg/ml lysostaphin solution. The mixture was then vortexed at room temperature for 1, 2, or 3 hours. After that, the same volume of SNP-PEG was mixed with the lysostaphin–PEG solution, and the mixture was continuously vortexed for 3 hours (Ravelo-Nieto *et al*., 2023).

Determining the antibacterial activity of lysostaphin and SNPs against MRSA strains and evaluating their synergistic potential

The MRSA isolates were used in three antibacterial activity experiments using lysostaphin alone with protein buffer as control that contains 10-mM imidazole and elution buffers contain 250-mM imidazole, SNPs alone using $AgNO_3$ solution as control, and lysostaphin-loaded SNPs with PEG as control.

The bacterial suspensions of MRSA strains were spread on the surface of the Mueller-Hinton agar. Holes of 6 mm in diameter were then created in the agar. Into these wells, 30 µl 2.38 mg/ml of the lysostaphin solution, 2.38-mg/ml SNPs solution, and SNPs–PEG–lysostaphin solution were added. This was followed by incubating the plates at 37°C for 24 hours. The inhibition zone diameters were read.

Statistical analysis

The data were recorded and presented as mean ± SE of the mean. A one-way ANOVA was utilized. The significance level was decided at less than 5% (Sheskin, 2004).

Ethical approval

The study was approved by the Committee of Research Ethics at the College of Veterinary Medicine, University of Al-Qadisyah, Al-Diwaniyah City, Iraq.

Results

Gene synthesis

In the current experiment, the complete nucleotide sequence of the lysostaphin gene was obtained from NCBI-GenBank (accession number: M15686.1). The synthetic lysostaphin gene, identified by the order name U591BHL130, was then constructed into the target cloning vector pET-28b (+) using BamHI/XhoI restriction enzymes and tagged with an N-Terminal polyhistidine-tag, as illustrated in the plasmid construction map.

The complete synthetic lysostaphin_pET-28b(+) clone was identified through digestion with the restriction enzymes BamHI and XhoI. The resulting fragments were separated using 1.5% agarose gel electrophoresis, as depicted in the accompanying.

Lysostaphin gene transformation identification

The BL21(DE3) chemically competent *E. coli* (C2527I) transformation cells exhibited positive lysostaphin_pET-28b(+) expression clones that displayed resistance to kanamycin antibiotic in LB agar plates at 37°C.

The positive transformed BL21(DE3) chemically competent *E. coli* bacterial colonies, which grew on selection LB agar plates with kanamycin antibiotics, were further subjected to the PCR technique for the detection of the presence of the recombinant lysostaphin_pET-28b(+) expression clone, as illustrated in Figure 1.

Recombinant lysostaphin protein expression

The results indicated that the highest concentration of purified lysostaphin protein (2381.20 µg/ml) was obtained with 1.0-mM IPTG at 25°C for 4–5 hours. Conversely, 0.25-, 0.5-, and 0.75-mM IPTG were induced lower concentrations at 37°C. The results of the lysostaphin protein concentrations are presented in Table 1.

The total extracted crude competent *E. coli* bacteria protein, negative control noninducible (−IPTG) competent *E. coli* bacterial protein, and purification column flow-through eluted 6× His-tagged lysostaphin proteins were separated by SDS-PAGE electrophoresis technique based on their molecular weight (kDa). The results of the SDS-PAGE are shown in Figure 2.

Reverse transcription real-time PCR (gene expression) of recombinant lysostaphin gene expression

Compared to the 0.25-mM IPTG-induced control, the data show that lysostaphin gene expression is the maximum at an IPTG concentration of 1 mM, with a fold change of 7.26 compared to the 0.25-mM IPTG-induced control (Figs. 3 and 4).

Antimicrobial activity of recombinant lysostaphin

The *in vitro* antimicrobial activity of recombinant lysostaphin against MRSA isolates was done by agar well diffusion method and the antibacterial activity was expressed by zone of bacterial growth inhibition around the wells. The control resulted in no zone of inhibition, while a 2.38-mg⁄ml concentration of recombinant lysostaphin showed a 12.33 ± 0.88 mm zone of inhibition.

Characterization of biosynthesized SNPs

Visible inspection

The SNPs were synthesized using *C. albicans*. When the $AgNO_3$ was added, the color was changed from pale yellow to yellowish brown. Later, the brown

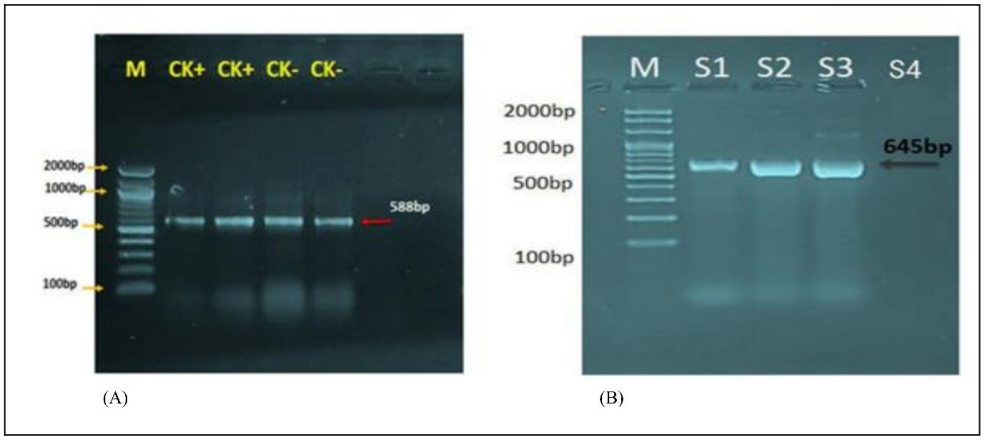

Fig. 1. Agarose gel electrophoresis of lysostaphin gene transformation. (**A**) The PCR product analysis of transformed BL21(DE3) chemically competent *E. coli* bacterial colonies. Lane (CK+) represents the *16SrRNA* gene in competent *E. coli* resistant to kanamycin antibiotic, while lane (CK−) represents the *16SrRNA* gene in competent *E. coli* sensitive to kanamycin antibiotic, both exhibiting a PCR product size of 588 bp. (**B**) Lane (S1–S3) shows positive lysostaphin gene clones in competent *E. coli* resistant to kanamycin antibiotic, each displaying a PCR product size of 645 bp. Lane (S4) indicates a negative lysostaphin gene clone in competent *E. coli* sensitive to kanamycin antibiotics, with a PCR product size of 645 bp.

Table 1. The concentration of eluted 6× His-tagged lysostaphin proteins by Bradford protein assay.

Group (0.25 IPTG mM)	OD	Concentrations (µg/ml)	mg/ml
S1	0.469	5913.92	5.91
W1	0.205	873.90	0.87
W2	0.074	22.25	**0.02**
E1	0.215	983.85	0.98
E2	0.155	419.75	0.42
Group (0.5 IPTG mM)			
S2	0.523	7492.16	7.49
W1	0.259	1543.37	1.54
W2	0.068	9.44	**0.01**
E1	0.219	1029.62	1.03
E2	0.169	530.85	0.53
Group (0.75 IPTG mM)			
S3	0.663	12449.56	12.45
W1	0.289	1995.62	2.00
W2	0.078	32.06	**0.03**
E1	0.262	1586.02	1.59
E2	0.175	582.29	0.58
Group (1.0 IPTG mM)			
S4	0.765	16848.13	16.85
W1	0.329	2687.87	2.69
W2	0.078	32.06	**0.03**
E1	0.312	2381.20	2.38
E2	0.195	770.32	0.77

E1 = Eluted protein purification by His-Taq magnetic beads supernatant lysostaphin protein; E2 = Eluted protein purification by His-Taq magnetic beads pallet lysostaphin protein; S = Crude protein the expression of total bacterial (BL21(DE3)) proteins of sample; W1 = Concertation protein in washing buffer in supernatant of sample; W2 = Concertation protein in washing buffer in pallet of sample.

color became darker with an increase in the incubation period as an indication of the formation of the SNPs (Fig. 5).

UV-vis spectroscopy

The features of the SNPs were identified by using a UV-vis spectrophotometer. The absorption spectrum is shown in Figure 6. A peak at 420 nm confirmed the SNP formation. As time goes, the absorbance increased, indicating ongoing reduction of silver ions and increasing the concentration of SNPs. Later, no peak detection was seen, which means that no further reaction occurred.

Scanning electron microscope (SEM)

The average size of the SNPs was reported as 127.05 nm. This value represents the average diameter of the nanoparticles. It is important to note that nanoparticles often exhibit a size distribution, meaning that individual particles may vary in size around this average. The relatively small size is typical for SNPs and advantageous for various applications, especially in catalysis and medical applications. The semi-spherical morphology observed in the SEM images suggests that the synthesis method has influenced the shape of the nanoparticles (Fig. 7).

The results of the FTIR analysis showed that after the interaction with silver ions or binding with SNPs, the secondary structure of proteins is unchanged. Furthermore, peptides and amino acids have been shown to create a coat around SNPs, inhibiting aggregation, according to IR spectroscopic investigations. According to these results, proteins and SNPs interact to protect proteins' structural integrity while aiding in the stability of the latter, which is essential for the functional uses of the former.

Antibacterial activity

The antibacterial activity of SNPs biosynthesized by cell biomass of *C. albicans* was tested against MRSA isolates. The SNPs efficiently inhibited the growth of these isolates and the zone of growth inhibition was 7.33 ± 1.2 mm. The results demonstrated that

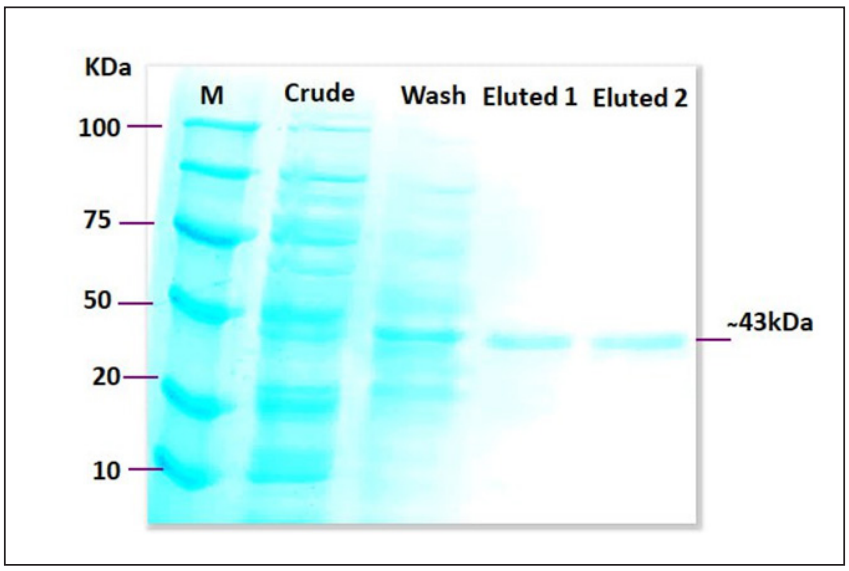

Fig. 2. SDS-PAGE image that showed protein expression production of recombinant lysostaphin where lane (M): protein marker ladder (100–10 kDa), lane (crude) showed the expression of total bacterial proteins, lane (wash) showed the expression of total bacterial proteins, and lane (Eluted1 and Eluted2) purified recombinant lysostaphin expression at (250-mM imidazole) after purification by His-Taq magnetic beads method at (~43 kDa) protein size.

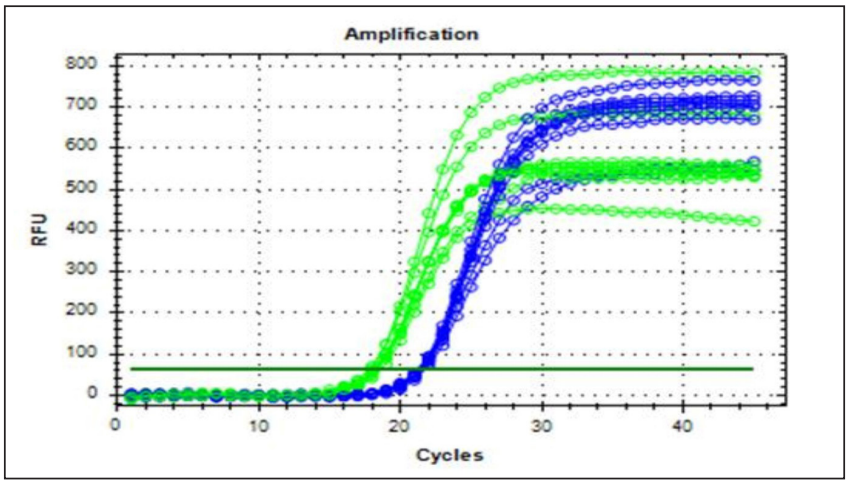

Fig. 3. Real-time amplification plots for the recombinant lysostaphin gene in IPTG inducer experimental BL21 isolates. The lysostaphin gene expression in *E. coli* cells stimulated with varying IPTG concentrations (0.25-, 0.5-, 0.75-, and 1-mM IPTG) is shown in the green graphs. The housekeeping *16sRNA* gene expression in *E. coli* cells stimulated with varying IPTG doses (0.25-, 0.5-, 0.75-, and 1-mM IPTG) is shown in blue plots.

the biosynthesized SNPs had antimicrobial activity against MRSA. In addition, the SNPs–PEG mixture was tested also to ensure that PEG has no antibacterial effect. The results have proven that there were no effects of the addition of PEG to biosynthesized SNPs.

Synergism evaluation of recombinant lysostaphin–nanoparticle combination

The combination of biosynthesized SNPs/PEG with lysostaphin exerted significant ($p < 0.05$) activity against tested MRSA bacteria, resulting in zone of growth inhibition of 20.33 ± 0.88 mm (Fig. 8 and Table 2).

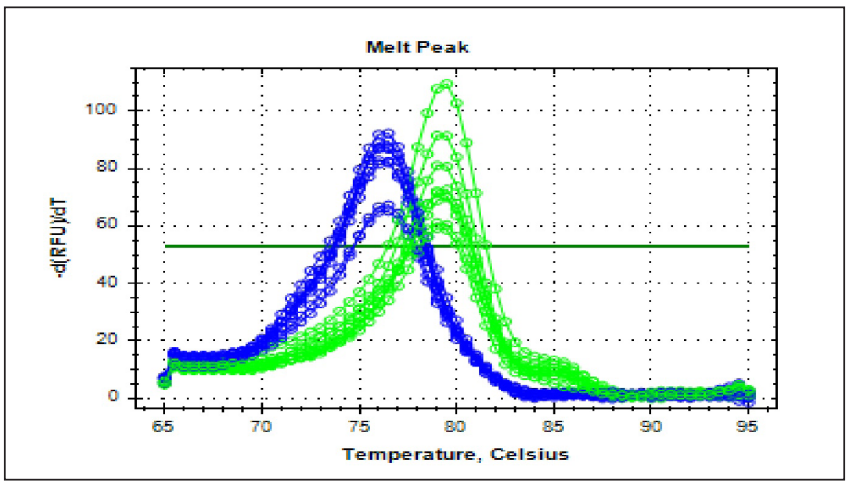

Fig. 4. The melting curve for recombinant lysostaphin gene in IPTG inducer experimental BL21 isolates. The green plots for the lysostaphin gene (*rLyso*) in *E. coli* cells induced with different concentrations of IPTG (0.25-, 0.5-, 0.75-, and 1-Mm IPTG). The blue plots for housekeeping *16SRNA* gene cells induced with different concentrations of IPTG (0.25-, 0.5-, 0.75-, and 1-Mm IPTG) showed qPCR product specificity melting peak at Tm:80°C and 78°C.

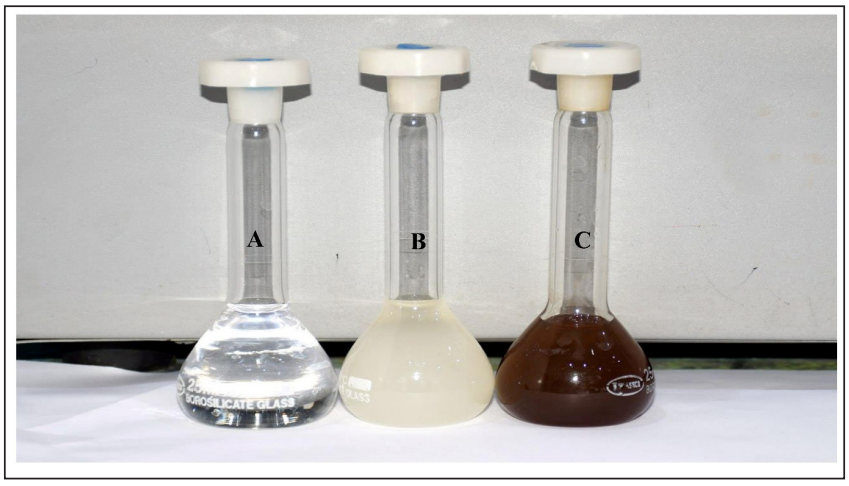

Fig. 5. Culture flasks containing 1-mM $AgNO_3$ solution (**A**), broth containing *C. albicans* cells (**B**), and mixture of *C. albicans* (**C**) with 1-mM $AgNO_3$.

These findings underscore that recombinant lysostaphin had promising antimicrobial properties, particularly when combined with synthesized SNPs, suggesting their potential application as effective antibacterial agents against MRSA.

Discussion

The successful outcomes of this research, focusing on the recombinant expression of lysostaphin in *E. coli* and the innovative fungal biosynthesis of SNPs using *C. albicans*. It contributes significantly to the field of antimicrobial therapies against resistant strains that have high risk and threatens human and animal health. These methodologies enhance understanding of microbial resistance and pave the way for a synergistic approach improving treatment against MRSA (Sheet, 2022).

The recombinant lysostaphin production was optimized to achieve maximal yield and functional activity agreement (Duman *et al*., 2019). The selected conditions of 25°C and 1-mM IPTG for induction provided a stable environment that likely promoted correct protein folding and minimized the formation of inactive aggregates. The current result is a critical consideration in recombinant protein production, where higher expression temperatures can accelerate cellular processes but at the risk of folding anomalies

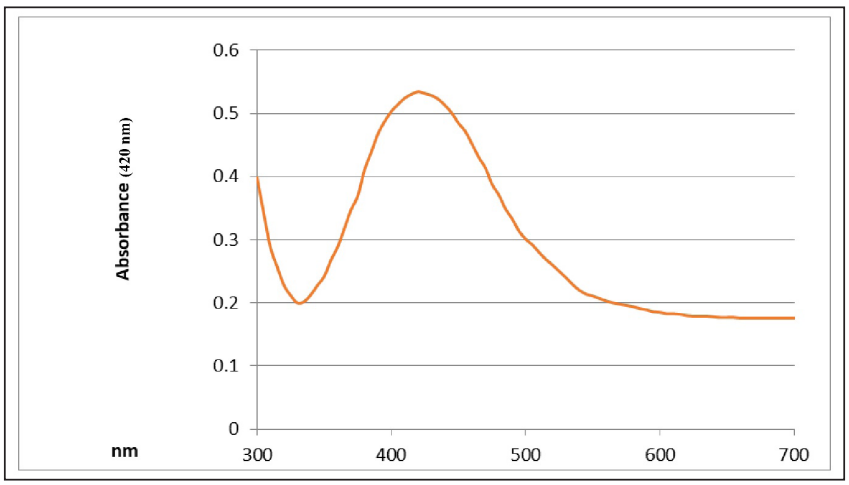

Fig. 6. UV-vis spectrophotometer analysis of biologically synthesized silver nanoparticles.

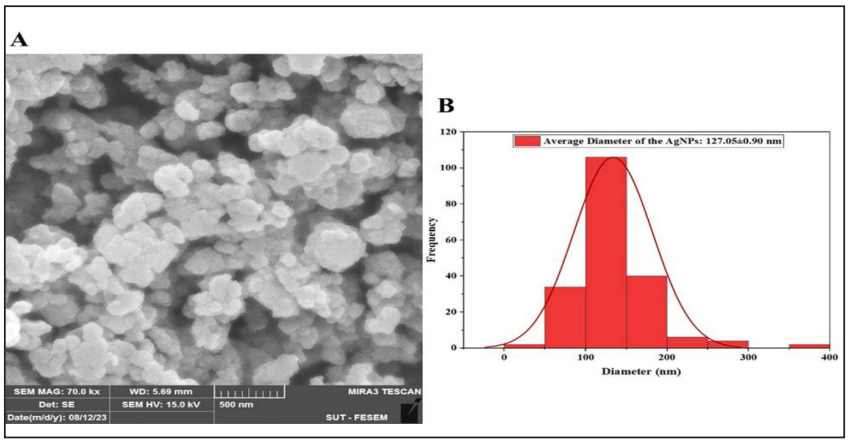

Fig. 7. Characterization of silver nanoparticles by SEM. (**A**) SEM image of silver nanoparticles biosynthesized from *C. albicans*. (**B**) Histogram average size SNPs.

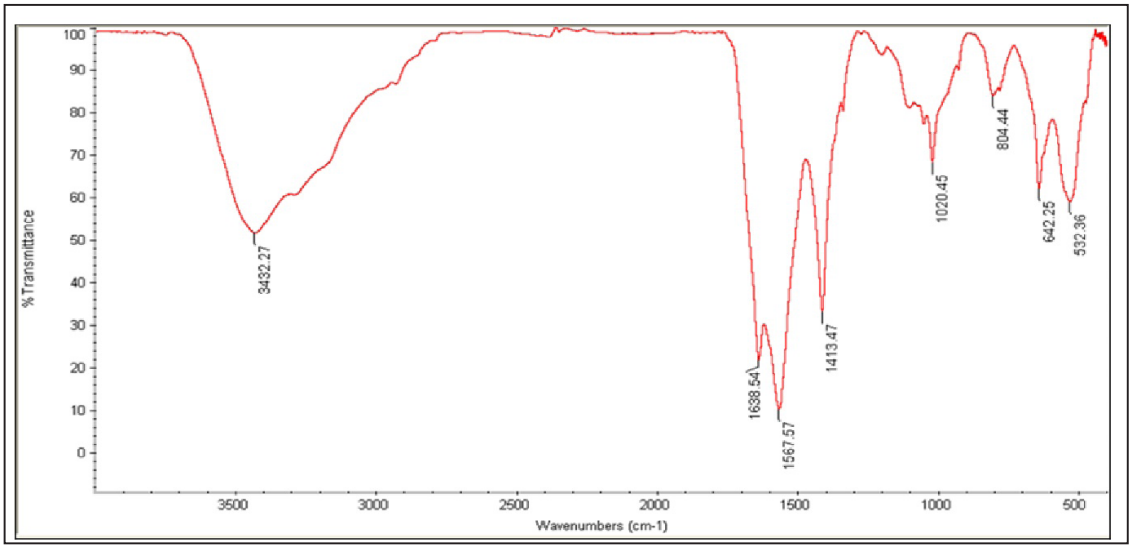

Fig. 8. FTIR spectrum of silver nanoparticles, synthesized by *C. albicans*, with distinct peaks.

Table 2. Anti-MRSA activity of tested materials represented by zone of growth inhibition.

Substance	Zone of inhibition (mm)
Lysostaphin	12.33 ± 0.88b
SNPs	7.33 ± 1.2a
SNPs–PEG–Lysostaphin	20.33 ± 0.88c
PEG	0 ± 0d
$AgNO_3$	0 ± 0d
LSD ($p < 0.05$)	2.82

LSD = least significant different; SNPs = silver nanoparticles; PEG = polyethylene glycol.

Different small letters mean significant ($p < 0.05$) differences between groups.

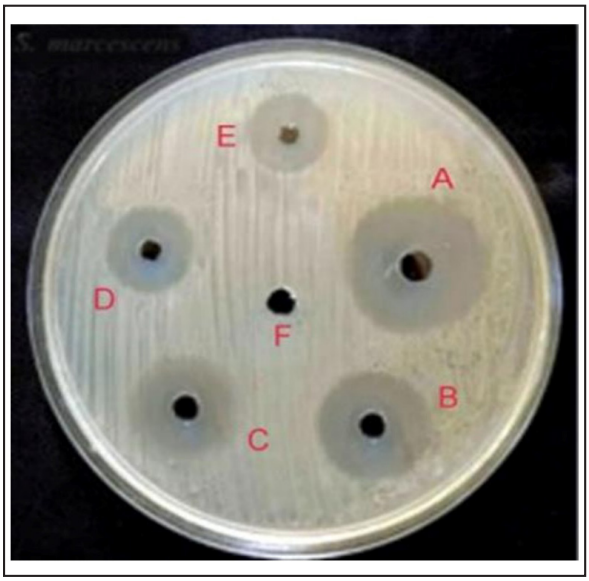

Fig. 9. Synergistic activity of tested material against MRSA strains. (**A**) NPs–PEG–lysostaphin), (B) lysostaphin, (C) lysostaphin–PEG, (D) SNPs, (E) SNPs–PEG, and (F) control (PEG).

and increasing metabolic burden on the host cells. Achieving a high degree of purity with His-tag purification not only confirms the effectiveness of the affinity chromatography technique but also ensures that the enzymatic activity of lysostaphin is preserved (Al Dujaily and Mahmood, 2021). This highlighted result is particularly vital considering the specific action of lysostaphin on the peptidoglycan layer of staphylococcal cell walls. This recombinant approach could significantly streamline production, enhancing the availability and consistency of lysostaphin for clinical and research applications (Duman-Özdamar *et al*., 2021).

One possibility is that the presence of the SNPs is facilitating lysostaphin access to its substrate binding sites on the bacterial cell wall. It has been reported that SNPs disrupt the plasma membrane of bacteria, although the mechanism is not known at this point, and may disrupt the electron transport chain in the cell membrane. One possibility is that SNPs non-specifically bind to membrane proteins and change their function, which results in increased permeability of the cell wall. We speculate that this increased permeability facilitates access of lysostaphin to its substrate (peptidoglycan), thereby enhancing the bacteriolytic activity of lysostaphin (Ahmed *et al*., 2022).

Furthermore, SNPs were shown to cause oxidative stresses within bacterial cells that promote disarray of cellular processes and weaken the bacterial cell physical structure, which in turn could sensitize bacteria to lysostaphin such that the combination posed a synergistic therapeutic effect far exceeding both therapeutic agents lysostaphin and SNPs individually (Norouzi *et al*., 2023).

The biosynthesis of SNPs using *C. albicans* introduces a sustainable and efficient nanoparticle production method (Hamida *et al*., 2021). The fungal synthesis process highlighted here is not only environmentally friendly but also advantageous due to the inherent capabilities of fungi to secrete proteins that naturally stabilize and cap nanoparticles, thus preventing aggregation and promoting colloidal stability (Norouzi *et al*., 2023). The formation of the SNPs was detected by the UV-vis spectrophotometer using the plasmon resonance phenomenon as evidence to detect size and shape (Rahimi *et al*., 2016). Many studies showed the formation of SNPs at 420-nm peak (Abdel-Rahim *et al*., 2017), which agrees with current study findings. The synthesized nanoparticles are observed as semi-spherical shapes, which are likely ideal for biomedical applications, including antimicrobial therapies. These physical characteristics ensure a large surface area relative to volume, enhancing the interaction between the nanoparticles and microbial cells, which is critical for the antimicrobial efficacy of SNPs (Balsam, 2017). The FTIR spectrum, displayed several distinct peaks at specific wavenumbers, each corresponding to different functional groups present in the biosynthesized SNPs. Notably, major peaks were observed at 3432.27 cm^{-1}, indicating O–H stretching vibrations, and at 1638.54 cm^{-1}, representing N–H bending vibrations (Oehler *et al*., 2024). These peaks suggest the presence of hydroxyl (OH) and amino (NH) groups, which are common in biological molecules and likely contribute to the stability and interaction of SNPs with biomolecules. The interaction between proteins and SNPs, as evidenced by FTIR analysis, not only preserves the structural integrity of proteins but also facilitates the stabilization of nanoparticles, which is crucial for their functional applications in various fields, including biomedicine and catalysis (Ahmed *et al*., 2022).

The two peaks at 3432.27 and 1638.54 cm^{-1} that are usually present in the FTIR spectra are normally assigned to specific functional groups of atoms that give rise to the stability, reactivity, and other characteristics of the nanoparticles (Gao *et al*., 2021).

The band at 3432.27 cm^{-1} is commonly attributed to O–H stretching vibrations, usually appearing with hydroxyl groups of water molecules or alcohol groups, which have been adsorbed on the surface of the nanoparticles. If these groups form hydrogen bonds, then they may create a hydration shell, which is known to enhance the colloidal stability of the nanoparticles, preventing aggregation. And, by forming hydrogen bonds with other molecules, it is possible that such groups imbue the nanoparticles with the ability to interact with biological molecules—potentially increasing biocompatibility and also enhancing their ability to recognize and bind to specific molecules on their target cells (Baranwal *et al*., 2023).

The peak at 1638.54 cm^{-1} corresponds to the amide I band, largely due to C=O stretching vibrations of proteins or peptides that could be capping or stabilizing the nanoparticles. The involvement of amide linkages indicates that peptides or proteins might be interacting with the nanoparticle surface by the carbonyl oxygen of the peptide bonds. This occurs not only to stabilize the nanoparticles in forming the protein corona but also dominantly contributes to their interaction with cell membranes and entry into cells (Bagheri *et al*., 2018).

Combining lysostaphin and biosynthesized SNPs demonstrated a remarkable synergistic effect on MRSA strains. This synergy is presumably due to the dual mechanisms of action where lysostaphin enzymatically breaches the cell wall (Douglas *et al*., 2022). At the same time, SNPs disrupt cellular membranes and internal structures, potentially through oxidative stress mechanisms (Zhongxi Gao, 2012). This study suggests that utilizing multiple antimicrobial mechanisms can effectively enhance bactericidal activity and potentially reduce the likelihood of developing resistance. MRSA, renowned for its capacity to acquire and be reluctant to accept antibiotics, presents a formidable challenge in clinical settings, and the combination therapy approach could offer a novel solution to overcome this (Radulescu *et al*., 2023).

The promising results from this study beckon further investigation, mainly through *in vivo* studies that could provide essential data on the efficacy and safety of the lysostaphin-SNP combination in animal models or clinical trials. In addition, exploring the stability, scalability, and delivery mechanisms of lysostaphin and SNPs will be necessary to transition from laboratory success to practical clinical applications. The highlighted result might include developing formulations that maintain the enzyme and nanoparticles' stability and activity under physiological conditions (Tantawy *et al*., 2022; Zhou *et al*., 2024).

Conclusion

This study effectively demonstrated the green synthesis of SNPs utilizing *C. albicans* and the cloning, expression, and purification of recombinant lysostaphin in *E. coli* against MRSA. SNP biosynthesis demonstrated a low-cost, eco-friendly method that uses the natural metabolic pathways found in fungi. These nanoparticles' stable and biocompatible features led to their characterization, indicating their potential for various biomedical applications. Lysostaphin and SNPs' combined antibacterial action against MRSA exhibits a solid synergistic effect, providing a potential therapeutic option for managing illness brought on by bacteria resistant to antibiotics. Subsequent investigations ought to concentrate on the clinical implementation of these discoveries, enhancing the dosage and delivery methods to optimize therapeutic effectiveness and reduce possible adverse reactions. This study paves the way for integrating biotechnological innovations in developing strategies against bacterial resistance, highlighting the interdisciplinary approach needed to address complex medical challenges.

Acknowledgments

The author is grateful to the College of Veterinary Medicine, University of Al-Qadysia, for all the facilities to achieve this study.

Conflict of interest

There is no conflict of interest in the current study.

Funding

The work received no financial assistance but relied on the authors' personal assets only.

Authors' contributions

Both authors participated equally in all parts of the study.

Data availability

The data presented in this study are available on request from the corresponding author.

References

Abdel-Rahim, K., Mahmoud, S., Ali, A.M., Almaary, K.S., Mustafa, M.A. and Husseiny, S.M. 2017. Extracellular biosynthesis of silver nanoparticles using Rhizopus stolonifer. Saudi J. Biol. Sci. 24(1), 208–216.

Ahmed, S.F., Mofijur, M., Rafa, N., Chowdhury, A.T., Chowdhury, S., Nahrin, M., Islam, A.B.M.S. and Ong, H.C. 2022. Green approaches in synthesising nanomaterials for environmental nanobioremediation: technological advancements, applications, benefits, and challenges. Environ. Res. 204(PA), 111967.

Al Dujaily, A.H. and Mahmood, A.K. 2021. The effectiveness of biogenic silver nanoparticles in the treatment of caprine mastitis induced by *Staphylococcus aureus*. Iraqi J. Vet. Sci. 35, 73–78.

Ali, S.A. and Chew, Y.W. 2015. FabV/Triclosan is an antibiotic-free and cost-effective selection system

for efficient maintenance of high- and medium-copy number plasmids in *Escherichia coli*. PLoS One 10(6), e0129547.

Bagheri, S., Yasemi, M., Safaie-Qamsari, E., Rashidiani, J., Abkar, M., Hassani, M., Mirhosseini, S.A. and Kooshki, H. 2018. Using gold nanoparticles in diagnosis and treatment of melanoma cancer. Artif. Cells Nanomed. Biotechnol. 46(sup1), 462–471.

Balsam, M.M. 2017. Myco-biosynthesis of silver nanoparticles by *Aspergillus niger* and evaluation of their antifungal activity in Dermatophytes spp. and Candida albicans. PhD diss., College of Medicine, University of Al-Qadisiyah, Iraq.

Baranwal, J., Barse, B., Di Petrillo, A., Gatto, G., Pilia, L. and Kumar, A. 2023. Nanoparticles in cancer diagnosis and treatment. Materials (Basel) 16(15), 5354.

Basavaraja, S., Balaji, S.D., Lagashetty, A., Rajasab, A.H. and Venkataraman, A.J. 2008. Extracellular biosynthesis of silver nanoparticles using the fungus *Fusarium semitectum*. Mater. Res. Bull. 43(5), 1164–1170.

Birla, S.S., Gaikwad, S.C., Gade, A.K. and Rai, M.K. 2013. Rapid synthesis of silver nanoparticles from *Fusarium oxysporum* by optimizing physicocultural conditions. Sci. World J. 2013, 795191.

Boksha, I.S., Lavrova, N.V., Grishin, A.V., Demidenko, A.V., Lyashchuk, A.M., Galushkina, Z.M. and Chernukha, M.I. 2016. *Staphylococcus simulans* recombinant lysostaphin: production, purification, and determination of antistaphylococcal activity. Biochemistry (Mosc.) 81(5), 502–510.

Ceotto-Vigoder, H., Marques, S.L., Santos, I.N., Alves, M.D., Barrias, E.S., Potter, A. and Bastos, M.C. 2016. Nisin and lysostaphin activity against preformed biofilm of *Staphylococcus aureus* involved in bovine mastitis. J. Appl. Microbiol. 121(1), 101–114.

Cumberland, S.A. and Lead, J.R. 2009. Particle size distributions of silver nanoparticles at environmentally relevant conditions. J. Chromatogr. A 1216(52), 9099–9105.

Dong, L., Liu, H., Meng, L., Xing, M., Wang, J., Wang, C., Chen, H. and Zheng, N. 2018. Quantitative PCR coupled with sodium dodecyl sulfate and propidium monoazide for detection of viable *Staphylococcus aureus* in milk. J. Dairy Sci. 101(6), 4936–4943.

Douglas, E.J., Alkhzem, A.H., Wonfor, T., Li, S., Woodman, T.J., Blagbrough, I.S. and Laabei, M. 2022. Antibacterial activity of novel linear polyamines against *Staphylococcus aureus*. Front. Microbiol. 13, 948343.

Duman-Özdamar, Z.E., Ünlü, A., Ünal, H., Woodley, J.M. and Binay, B. 2021. High-yield production of active recombinant *S. simulans* lysostaphin expressed in *E. coli* in a laboratory bioreactor. Protein Expr. Purif. 177, 105753.

Duman, Z.E., Ünlü, A., Çakar, M.M., Ünal, H. and Binay, B. 2019. Enhanced production of recombinant *Staphylococcus simulans* lysostaphin using medium engineering. Prep. Biochem. Biotechnol. 49(5), 521–528.

Faghihzadeh, F., Anaya, N.M., Schifman, L.A. and Oyanedel-Craver, V. 2016. Fourier transform infrared spectroscopy to assess molecular-level changes in microorganisms exposed to nanoparticles. Nanotechnol. Environ. Eng. 1, 1–16.

Fagundes, H., Barchesi, L., Nader Filho, A., Ferreira, L.M. and Oliveira, C.A. 2010. Occurrence of *Staphylococcus aureus* in raw milk produced in dairy farms in São Paulo state, Brazil. Braz. J. Microbiol. 41, 376–380.

Fang, W., Wu, J., Cheng, M., Zhu, X., Du, M., Chen, C. and Pan, W. 2023. Diagnosis of invasive fungal infections: challenges and recent developments. J. Biomed. Sci. 30(1), 42.

Gao, Q., Zhang, J., Gao, J., Zhang, Z., Zhu, H. and Wang, D. 2021. Gold nanoparticles in cancer theranostics. Front. Bioeng. Biotechnol. 9, 647905.

Gomes, F. and Henriques, M. 2016. Control of bovine mastitis: old and recent therapeutic approaches. Curr. Microbiol. 72, 377–382.

Gonçalves, J.L., Kamphuis, C., Martins, C.M., Barreiro, J.R., Tomazi, T., Gameiro, A.H., Hogeveen, H. and Dos Santos, M.V. 2018. Bovine subclinical mastitis reduces milk yield and economic return. Livest. Sci. 210, 25–32.

Grishin, A.V., Konstantinova, S.V., Vasina, I.V., Shestak, N.V., Karyagina, A.S. and Lunin, V.G. 2020. A simple protocol for the determination of lysostaphin enzymatic activity. Antibiotics 9(12), 917.

Guardabassi, L., Butaye, P., Dockrell, D.H., Fitzgerald, J.R. and Kuijper, E.J. 2020. One health: a multifaceted concept combining diverse approaches to prevent and control antimicrobial resistance. Clin. Microbiol. Infect. 26(12), 1604–1605.

Hamida, R.S., Ali, M.A., Goda, D.A. and Redhwan, A. 2021. Anticandidal potential of two cyanobacteria-synthesized silver nanoparticles: effects on growth, cell morphology, and key virulence attributes of Candida albicans. Pharmaceutics 13(10), 1688.

Hema, J.A., Malaka, R., Muthukumarasamy, N.P., Sambandam, A., Subramanian, S. and Sevanan, M. 2016. Green synthesis of silver nanoparticles using Zea mays and exploration of its biological applications. IET Nanobiotechnol. 10(5), 288–294.

Ibrahim, A., Peyclit, L., Abdallah, R., Khelaifia, S., Chamieh, A., Rolain, J.M. and Bittar, F. 2021. Sca medium: a new culture medium for the isolation of all Candida auris clades. J. Fungi 7(6), 433.

Ivak, K.J. and Schmittgen, T.D. 2001. Math. Methods 25(4), 402–408.

Jayakumar, J., Kumar, V.A., Biswas, L. and Biswas, R. 2021. Therapeutic applications of lysostaphin

against *Staphylococcus aureus*. J. Appl. Microbiol. 131(3), 1072–1082.

Khandel, P. and Shahi, S.K. 2018. Mycogenic nanoparticles and their bio-prospective applications: current status and future challenges. J. Nanostruct. Chem. 8, 369–391.

Lekha, D.C., Shanmugam, R., Madhuri, K., Dwarampudi, L.P., Bhaskaran, M., Kongara, D., Tesfaye, J.L., Nagaprasad, N., Bhargavi, V.N. and Krishnaraj, R. 2021. Review on silver nanoparticle synthesis method, antibacterial activity, drug delivery vehicles, and toxicity pathways: recent advances and future aspects. J. Nanomater. 2021, 4401829.

Norouzi, E., Hosseini, S.M., Asghari, B., Mahjoub, R., Nazarzadeh Zare, E., Shahbazi, M.A., Kalhori, F. and Arabestani, M.R. 2023. Anti-biofilm effect of ampicillin-loaded poly (lactic-co-glycolic acid) nanoparticles conjugated with lysostaphin on methicillin-resistant Staphylococcus aureus. Can. J. Infect. Dis. Med. Microbiol. 2023, 4627848.

Oehler, J.B., Rajapaksha, W. and Albrecht, H. 2024. Emerging applications of nanoparticles in the diagnosis and treatment of breast cancer. J. Pers. Med. 14(7), 723.

Pinzaru, I., Coricovac, D., Dehelean, C., Moacă, E.A., Mioc, M., Baderca, F., Sizemore, I., Brittle, S., Marti, D., Calina, C.D. and Tsatsakis, A.M. 2018. Stable PEG-coated silver nanoparticles: a comprehensive toxicological profile. Food Chem. Toxicol. 111, 546–556.

Radulescu, D.M., Surdu, V.A., Ficai, A., Ficai, D., Grumezescu, A.M. and Andronescu, E. 2023. Green synthesis of metal and metal oxide nanoparticles: a review of the principles and biomedical applications. Int. J. Mol. Sci. 24(20), 15397.

Rahimi, G., Alizadeh, F. and Khodavandi, A. 2016. Mycosynthesis of silver nanoparticles from Candida albicans and its antibacterial activity against *Escherichia coli* and *Staphylococcus aureus*. Trop. J. Pharm. Res. 15, 371–375.

Ravelo-Nieto, E., Cifuentes, J., Ruiz Puentes, P., Rueda-Gensini, L., Quezada, V., Ostos, C., Muñoz-Camargo, C., Reyes, L.H., Duarte-Ruiz, A. and Cruz, J.C. 2023. Unlocking cellular barriers: silica nanoparticles and fullerenol conjugated cell-penetrating agents for enhanced intracellular drug delivery. Front. Bioeng. Biotechnol. 11, 1184973.

Rosenberg, I.M. 1996. Electrophoretic techniques. In Protein analysis and purification: benchtop techniques. Boston: Birkhäuser. 63, 265–290.

Shahid, M. and Khan, M.S. 2020. Pesticide-induced alteration in proteins of characterized soil microbiota revealed by sodium dodecyl sulphate–polyacrylamide gel electrophoresis (SDS-PAGE). J. Proteins Proteomics 11(1), 1–9.

Sheet, O.H. 2022. Molecular detection of mecA gene in methicillin-resistant *Staphylococcus aureus* isolated from dairy mastitis in Nineveh governorate, Iraq. Iraqi J. Vet. Sci. 36(4), 939–943.

Sheskin, D.J. 2004. Handbook of parametric and nonparametric statistical procedures. 3rd ed. Boca Raton: Chapman & Hall/CRC, pp: 1–77.

Szweda, P., Pladzyk, R., Kotlowski, R., & Kur, J. 2001. Cloning, expression, and purification of the *Staphylococcus simulans* lysostaphin using the intein-chitin-binding domain (CBD) system. Protein. Expr. Purif. 22(3), 467–471.

Tantawy, E., Schwermann, N., Ostermeier, T., Garbe, A., Bähre, H., Vital, M. and Winstel, V. 2022. *Staphylococcus aureus* multiplexes death-effector deoxyribonucleosides to neutralize phagocytes. Front. Immunol. 13, 847171.

Timmerman, C.P., Mattsson, E., Martinez-Martinez, L., De Graaf, L., Van Strijp, J.A., Verbrugh, H.A., … Fleer, A. 1993. Induction of release of tumor necrosis factor from human monocytes by staphylococci and staphylococcal peptidoglycans. Infect. Immun. 61(10), 4167–4172.

Xie, H., Liu, Y., An, H., Yi, J., Li, C., Wang, X. and Chai, W. 2022. Recent advances in prevention, detection and treatment in prosthetic joint infections of bioactive materials. Front. Bioeng. Biotechnol. 10, 1053399.

Zhongxi, G. 2012. Sodium nitroprusside (SNP) alleviates the oxidative stress induced by NaHCO3 and protects chloroplast from damage in cucumber. Afr. J. Biotechnol. 11(27), 6974–6982.

Zhou, Y., Guo, L., Dai, G., Li, B., Bai, Y., Wang, W., Chen, S. and Zhang, J. 2024. An overview of polymeric nanoplatforms to deliver veterinary antimicrobials. Nanomaterials 14(4), 341.